





Techno-economic analysis of the use of atomic layer deposited transition metal oxides in silicon heterojunction solar cells

Nathan L. Chang¹  | Geedhika K. Poduval¹ | Borong Sang¹ | Kean Khoo¹ | Michael Woodhouse² | Fred Qi¹ | Mohammad Dehghanimadvar¹  | Wei Min Li³ | Renate J. Egan¹  | Bram Hoex¹ 

¹University of New South Wales, Sydney, New South Wales, Australia

²National Renewable Energy Labs, Golden, Colorado, USA

³Jiangsu Leadmicro Nano-Equipment Technology Ltd., Wuxi, China

Correspondence

Nathan L. Chang and Bram Hoex, University of New South Wales, Sydney, NSW 2052, Australia.

Email: n.chang@unsw.edu.au and b.hoex@unsw.edu.au

Funding information

Australian Renewable Energy Agency, Grant/Award Number: 2017/RND007

Abstract

The industry for producing silicon solar cells and modules has grown remarkably over the past decades, with more than a 100-fold reduction in price over the past 45 years. The main solar cell fabrication technology has shifted over that time and is currently dominated by the passivated emitter and rear cell (PERC). Other technologies are expected to increase in market share, including tunnel-oxide passivated contact (TOPCon) and heterojunction technology (HJT). In this paper, we examine the cost potential for using atomic layer deposition (ALD) to form transition metal oxide (TMO) layers (MoO_x, TiO_x and aluminium-doped zinc oxide [AZO]) to use as lower cost alternatives of the p-doped, n-doped and indium tin oxide (ITO) layers, respectively, the layers normally used in HJT solar cells. Using a bottom-up cost and uncertainty model with equipment cost data and process experience in the lab, we find that the production cost of these variations will likely be lower per wafer than standard HJT, with the main cost drivers being the cost of the ALD precursors at high-volume production. We then considered what efficiency is required for these sequences to be cost effective in \$/W and discuss whether these targets are technically feasible. This work motivates further work in developing these ALD TMO processes to increase their efficiency towards their theoretical limits to take advantage of the processing cost advantage.

KEYWORDS

atomic layer deposition, passivating contact solar cell, techno-economic analysis, transition metal oxide

1 | INTRODUCTION

The production and market for photovoltaics (PV) modules have increased in scale and reduced in cost significantly over the past decades, as shown in industry reports such as the International Technology Roadmap for Photovoltaic (ITRPV),¹ which estimated

cumulative shipments of 789 GW at the end of 2020, and a more than 100-fold reduction in market price (in \$/W) over a 45-year period. Demand for PV modules is expected to remain strong.²

The technology used to produce the solar cells in these modules continues to change over time. Figure 1 shows the current and projected market share of different silicon cell technologies of two industry

This is an open access article under the terms of the [Creative Commons Attribution-NonCommercial](https://creativecommons.org/licenses/by-nc/4.0/) License, which permits use, distribution and reproduction in any medium, provided the original work is properly cited and is not used for commercial purposes.

© 2022 The Authors. Progress in Photovoltaics: Research and Applications published by John Wiley & Sons Ltd.

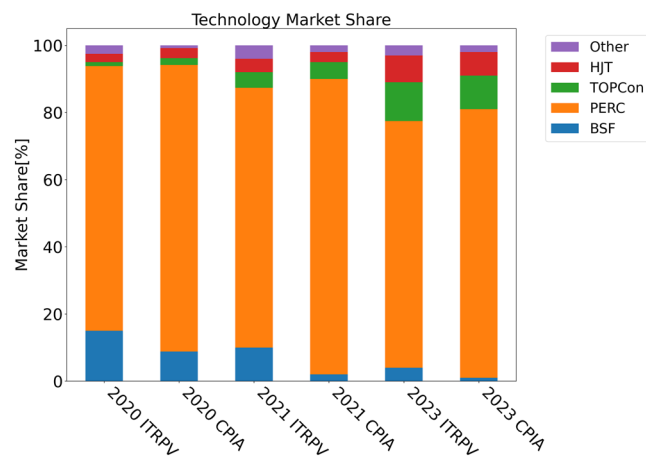


FIGURE 1 Technology market share reported in ITRPV and CPIA for 2020 and projected years

roadmaps—the ITRPV¹ produced in Europe and CPIA³ produced in China. The once-dominant aluminium back surface field (Al-BSF) technology was a small fraction of production in 2020, and the market has been taken over by the passivated emitter, rear-contact (PERC) technology. These roadmaps predict an increasing market share for passivated contact technologies such as tunnel-oxide passivated contact (TOPCon) and heterojunction technology (HJT, sometimes abbreviated SHJ). The reason for interest in these passivating contact technologies is their higher efficiency potential because of improved full area surface passivation and the avoidance of a silicon-metal contact, leading to reduced surface recombination and higher voltages.⁴ Many research groups and manufacturers are developing these technologies, with high efficiencies reported at both lab and industrial scale. A time series of high lab efficiencies are summarized in Figure 2, with references in the caption. Industrial-scale records at time of writing are 25.2% for TOPCon⁵ and 26.3%⁶ for SHJ solar cells.

In this work, we focus on a related group of as yet uncommercialized technologies—those utilizing transition metal oxides (TMOs) as part of passivating electron and hole contacts.

For research groups developing passivated contact technologies, it is important to consider economic factors, as the industry is not only focused on efficiency but also considers the cost (\$/cell or \$/W). It is helpful in this case to carry out cost analysis of processes that are under development to understand the commercial potential as well as barriers to adoption. The insights from such analysis can help focus research on the key factors that must be improved in order that the new technology can become competitive.

In this work, we review solar cell manufacturing bottom-up cost data from the National Renewable Energy Labs (NREL), including a recent 2021 update. We build on this to estimate the cost of possible implementations of novel TMO layers in passivating electron and hole contacts and as transparent conductive oxide (TCO) layers. We first outline the technical advantages and disadvantages of these structures, including the potential solar cell efficiency. We then complete a cost analysis of a range of proposed structures to identify process

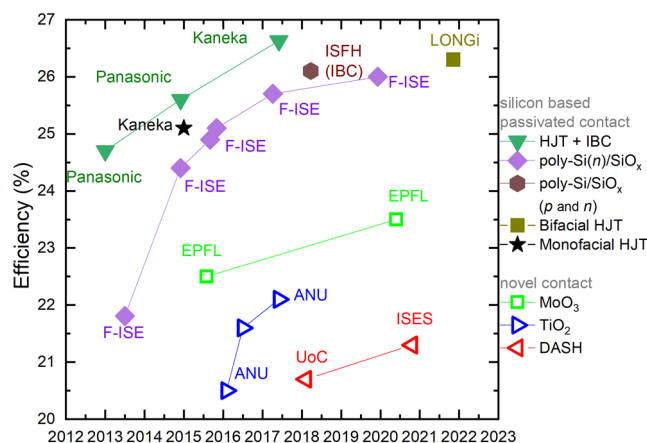


FIGURE 2 Progress in solar cell efficiencies using HJT,^{7–9} TOPCon,^{10–15} IBC,¹⁶ and DASH^{17,18} passivated contacts and TMO based passivating electron^{19,20} and hole contacts^{21–24}

cost improvement and efficiency improvement targets for these technologies.

2 | NREL BOTTOM-UP COST DATA FOR ALTERNATIVE SOLAR CELL TECHNOLOGIES

The NREL group has published process step cost data for many PV production sequences using a bottom-up cost of ownership model. For example, in 2019, Woodhouse et al²⁵ analysed the cost of manufacture in 2018 for polysilicon, wafer, solar cell and module fabrication. For solar cell fabrication, two industrial sequences were included, Al-BSF and PERC, and three emerging sequences, n-PERT, HJT, and interdigitated back contact (IBC). The NREL methodology is to seek detailed data from equipment suppliers and PV manufacturers to give the most accurate cost result possible, but for reasons of confidentiality, the exact bottom-up input parameters are not revealed.

In this paper, we provide recent (2021) data from the NREL cost models for PERC, n-PERT and HJT sequences as well as new analysis of the TOPCon structure. These data have been provided by NREL in summary form based on the most up-to-date data from the NREL model as at December 2021. The detailed step-by-step cost data in graphical and tabular form are shown in the supporting information, Section S1. In Figure 3, we show a summary of the 2018 and 2021 NREL cost data as well as cost data obtained from PV Infolink.²⁶

For each of the technologies shown, there has been an improvement in solar cell efficiency and a reduction in cost over time. However, in 2018 and 2021, advanced solar cell technologies such as n-PERT, HJT and TOPCon have higher manufacturing cost per watt than the market-leading PERC technology. In particular, HJT is higher cost because of the need for large amounts of expensive low-temperature silver paste and a higher depreciation cost from the expensive PECVD equipment. We note that in the market, the manufacturing cost in \$/W is not the only determining metric for

competitiveness. For example, (i) solar cells with higher efficiency will result in higher efficiency modules which require comparatively less space and system mounting hardware and so a lower balance of systems cost, and (ii) modules that degrade more slowly or have lower failure rates will have increased electricity production, reducing the levelized cost of electricity (LCOE).

Examining the NREL cost data between 2018 and 2021: (i) There have been significant reductions in depreciation costs for PERC, n-PERT and HJT. This is due to decreases in equipment cost, in particular because of an increasing number of lower cost Chinese based equipment suppliers, as well as improvements in equipment throughput. (ii) Metallization paste costs reduced significantly for PERC due to reductions in usage (g/wafer), less so for n-PERT. There was an increase for HJT due to a cost update for the low-temperature paste cost being significantly higher than the cost of the input silver (iii) other materials costs are fairly similar between technologies and have not changed significantly and (iv) for labour cost, the headcount per production capacity decreased due to increases in equipment throughput, but this was counteracted by an increase in the assumption for labour rates in China.

PV Infolink has 2021 estimated manufacturing cost data for PERC, TOPCon and HJT, but the data are not broken down into individual cost categories. The NREL cost results are broadly in line with this, with the advantage of having a detailed step-by-step resolution as well as categorization into cost components. We start with this NREL data as a strong basis to build additional cost estimates applied to novel TMO solar cell architectures.

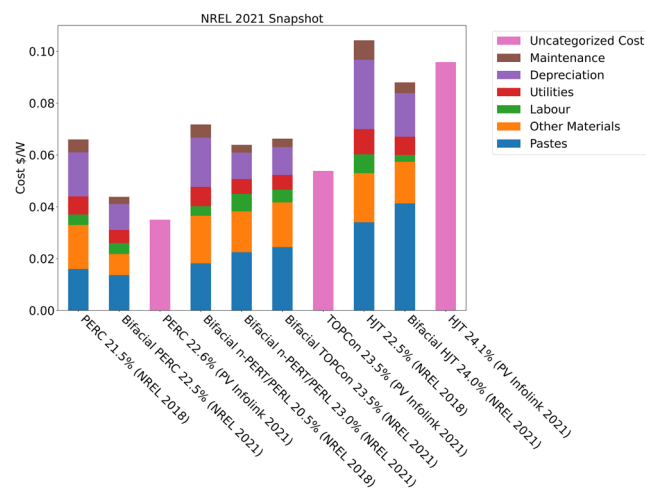


FIGURE 3 A comparison of NREL cost data for the cell conversion cost of alternate solar cell technologies from 2018 and 2021. The detailed breakdown of 2021 data is shown in the supporting information, Section S1. Year 2018 data are from Woodhouse et al.²⁵ Also shown are total cost estimates from PV Infolink²⁶

3 | SOLAR CELL ARCHITECTURES EMPLOYING TMOs

The data from industry roadmaps indicate increasing manufacturing volumes for TOPCon and HJT.^{1,3} Within research institutes, there is interest in exploring possibilities to increase the efficiency or reduce the cost of these types of solar cells. Recently, TMOs have emerged as an appealing alternative for doped silicon films in passivating contacts due to their relatively high bandgap resulting in significantly lower parasitic optical absorption compared to heavily doped a-Si layers on the front and rear sides of HJT solar cells. To compensate for the low lateral conductivity of a-Si, indium tin oxide (ITO) is usually used as the TCO on these structures, but alternative TMO layers are of interest if they can reduce reliance on the high-cost indium

3.1 | TMOs—benefits for silicon solar cells

Although HJT structures have achieved high efficiency by employing doped a-Si layers that provide excellent surface passivation, a high parasitic optical absorption of a-Si layers limits the photo-generated current and thus limits the performance of the solar cells.^{27,28} TMOs usually have a wider bandgap than doped a-Si, resulting in less parasitic absorption. TMOs can be used in both passivating electron and hole contacts due to their wide range of work functions and band alignment offsets.²⁹ In Figure 4A, we show various TMOs and their relative band alignment to silicon, and in Figure 4, we show a band diagram of these layers in a full solar cell structure. When applying MoO_x on silicon, the significant difference in workfunction results in band bending in silicon, thereby increasing the hole concentration at the interface resulting in a high hole conductivity and low electron conductivity. In combination with an a-Si interface passivation layer, this results in a very effective passivating hole contact with a record efficiency of 23.5% to date.²³ In the case of TiO_x, which has been reported to be an effective electron transport layer on silicon with excellent passivation effect,^{30,31} we can see that there is a close band offset with the conduction band of silicon, while there is a large discrepancy in the valence band offset, providing high conductivity to electrons transporting from TiO_x into the silicon bulk, while holes are effectively repelled. It is also verified that the passivation effect on the silicon surface can be preserved by the TiO_x/i-a-Si:H stack after an annealing process of up to 300°C, while providing a low contact resistivity of around 15 mΩ cm².^{32–34} TCOs are often used as part of the passivating contact structure to compensate for the relatively low lateral conductivity of the thin TMO or doped a-Si layers used. In addition, the TCO layer can serve as an antireflection coating, as in the case of a HJT solar cell.

Because of these potential advantages, there has been interest in demonstrating the use of these layers in silicon solar cells. Titanium oxide (TiO_x),^{20,38} niobium oxide (NbO_x)³⁹ and tantalum oxide (TaO_x)⁴⁰ have been used in passivating electron contacts, while molybdenum oxide (MoO_x),²³ tungsten oxide (WO_x),⁴¹ vanadium oxide (VO_x)⁴² and chromium oxide (CrO_x)⁴³ have been used in passivating hole contacts

FIGURE 4 (A) Band alignment of various passivation layers^{35,36} and TMOs studied in this work. They include the band energies of MoO_x for hole-selectivity,²⁹ TiO_x for electron-selectivity,³⁵ and ITO and ZnO³⁷ as TCOs. (B) Band diagram of a solar cell structure incorporating proposed TMO layers

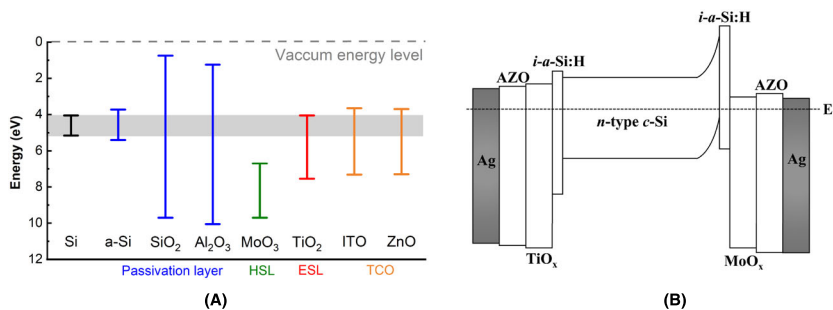


TABLE 1 TMO deposition methods and their advantages and disadvantages

	ALD (batch)	ALD (spatial)	PECVD	Sputtering	Thermal evaporation
Uniformity	Superior	Superior	Good	Very good	Poor
Substrate temperature (°C)	50–100	20–200	200–300	20–200	50–100
Deposition rate (Å/s)	0.1–1	1–10	10–100	1–10	1–20
Impurity level	Very low	Very low	Very low	Low	high

Note: Exact values for uniformity and impurity levels will change according to equipment design, but commercially equipment uniformity specifications of >98% for ALD⁸² and >95% for both PECVD⁸³ and sputtering⁸⁴ have been found.

Source: Data obtained and adapted from French et al.⁸¹

in silicon solar cells to replace the highly doped a-Si layers in HJT structures. ITO, doped indium oxide [In₂O₃:X (X are dopants such as H,⁴⁴ Sn⁴⁵ and Zn⁴⁶)], and doped zinc oxide (ZnO: Al,^{47,48} B⁴⁹ and Ga⁵⁰) have been considered as TCOs for solar cell structures.

Figure 2 details high efficiencies achieved using MoO_x and TiO_x in the laboratory. A full area atomic layer deposited (ALD) TiO_x was successfully applied in an n-type silicon solar cell device as an electron selective contact and achieved an efficiency of 22.1%.⁵¹ More recently, a 23.5% conversion efficiency was reported for a HJT structure with MoO_x instead of boron-doped a-Si. A higher short-circuit current density was achieved in the solar cell with MoO_x than the standard HJT solar cell, due to the lower parasitic absorption in the MoO_x, with efficiency equivalency between the standard HJT and MoO_x structures.²³ The fundamental limit imposed by TMO passivating electron and hole contacts is above 27%, indicating that there is still ample room for improvement.⁴

Various TMOs have been explored as an indium free TCO, but AZO has the closest electro-optical properties to ITO.^{47,52–54} Tests have shown that sputtered AZO has the same efficiency potential as ITO.^{55,56} Other reports show that ALD-deposited AZO can give equivalent efficiency to ITO for HJT solar cells when used on either the front, rear, or both sides of the solar cell, with efficiency values of 23%⁵⁷ and 22.5%.⁵⁸ Efficiency parity has also been shown for large area solar cells, with efficiency values over 21.1%.⁵⁹

Some groups have applied passivating contacts with TMOs for both the electron and hole contacts. These structures are referred to as dopant-free asymmetric heterocontacts (DASH) solar cells.^{4,60–68} A fundamental and theoretical investigation suggest that the band structure is suitable for next-generation high-efficiency solar cells.⁶⁹ Recently, Bullock et al. demonstrated a solar cell with an electron and

hole selective TMO contact—TCO/MoO_x (thermally evaporated)/i-a-Si:H/c-Si/i-a-Si:H/TiO_x (ALD)/LiF/Al that resulted in an efficiency of 20.7%.¹⁷ Although the TCO used was ITO, AZO is expected to have efficiency parity to ITO when implemented in DASH structures.^{18,70}

When considering the cost and efficiency potential of these structures, it is important to identify a benchmark efficiency for standard HJT solar cells as a comparison. We have selected the 26.3% efficiency HJT solar cell,⁶ which is the highest lab efficiency we have identified for non-IBC HJT solar cells.

3.2 | TMO fabrication methods

There are variety of techniques to deposit thin TMO layers, with a comparison of methods summarized in Table 1. Sol-gel spin coating is widely used in depositing TMOs such as ZnO and TiO_x as transport layers in organic solar cells, perovskite solar cells or dye-sensitized solar cells. However, it is usually challenging to achieve a uniform ultra-thin layer such as required in passivating contact layers for silicon solar cells with only a few nanometres.^{71,72} Thermal evaporation and plasma-enhanced chemical vapour deposition (PECVD) are also popular methods to deposit thin TMO layers in solar cells.^{73–75} Nonetheless, its fast surface reaction rate and shadowing effects limits the conformality of the films.⁷⁶ Of particular interest is ALD, a self-limiting process that can grow TMO thin films of high quality and with fine control of the uniformity and thickness.^{77,78} Moreover, compared to other deposition methods, ALD can grow pin-hole free materials on large areas, which makes it an appealing alternative for manufacturing.⁷⁹ The ALD technique is attracting more attention in the solar cell industry because of these advantages. ALD Al₂O₃ has already

successfully been introduced in PERC solar cell production with superior performance, as well as lower processing cost, which is crucial for industrialisation.⁸⁰ Within the PV industry, batch ALD is favoured over spatial ALD, and this trend is expected to continue.¹

Compared to the TMO layers in passivating contacts, optimized TCO layers are significantly thicker (~75 nm) to ensure high bulk conductivity while avoiding excessive parasitic absorption and having good antireflective properties. The industrial standard deposition technique for ITO layers is magnetron sputtering.⁸⁵ Sputtering results in the desired layer quality while being economical for thicker layers, but it also induces near-surface defects. On the other hand, ALD causes negligible process-induced interface defects,⁸⁶ offers high control of the film thickness and composition. Nonetheless, its slow growth rate is still a major economic bottleneck.

ALD growth of indium oxides has additional challenges of high precursor cost, low growth rate and long nucleation time.^{44,87–91} On the other hand, ALD of ZnO is a mature process, and the commonly used Zn precursor is a low-cost chemical that is readily available.^{92,93} Moreover, low-temperature growth of TCO on temperature-sensitive a-Si can be achieved by ALD grown ZnO at temperatures as low as 100°C.^{94,95}

With the performance potential of TMOs and a high quality of deposition using ALD, these materials hold promise for industrial applications in HJT devices. Hence, we examine the feasibility of applying ALD TMOs into industry from a perspective of techno-economic analysis. Four solar cell architectures employing TMO layers are proposed based on a standard HJT solar cell structure, as shown in Figure 5. Seq A is a standard HJT, Seq B, C and D replace the p-doped, n-doped and ITO layers with MoO_x, TiO_x and AZO, respectively. Seq E combines all three ALD TMO layers into one structure. The process sequence assumed for each of these is shown in Table S5.

4 | COST ANALYSIS

4.1 | Methods

In order to estimate the cost of implementing the ALD TMO layers in high-volume production, a cost model using a Monte Carlo uncertainty approach was used as described in previous work.⁹⁶ In brief,

the method is a bottom-up cost of ownership model that allows for Low, Med and High values for each input instead of assuming a single number. The model then uses a Monte Carlo approach to sample each input variable using a two-half log-normal distribution based on the uncertainty values (Low = 10th percentile, Med = median, High = 90th percentile). The two-half distribution allows the Med value to be the median of the distribution, and the log-normal distribution avoids the generation of negative numbers. Repeating this process many times, the output of the analysis is a distribution of calculated costs together with an understanding of the key factors that lead to cost uncertainty. The Monte Carlo model was run using a python script on a Windows notebook computer. This method is particularly useful when processes are being developed in the lab, where exact data are difficult to obtain, such as (i) material cost and usage at production volumes, (ii) equipment cost and throughput, and (iii) production solar cell efficiencies.

4.2 | Assumptions for ALD TMO deposition

The cost of growing ALD layers is comprised of two main components—(i) the cost to purchase, maintain and operate the equipment (including depreciation of the purchase price, and electricity, labour, and maintenance expenses); and (ii) the cost of the materials, including the ALD precursors.

The cost of equipment is based on data from an equipment manufacturer—Leadmicro's list price data for the KF Series (KF20000S) industrial batch type ALD system. This fully automated system with auto-guided vehicle and manufacturing execution systems is optimized to produce high-quality ultra-thin aluminium oxide (Al₂O₃) for the PERC solar cell rear surface passivation.⁸² This system can be operated between 150°C and 300°C for the growth of Al₂O₃ and other oxides (SiO₂, TiO_x, ZnO) and has a 20,000 wafer/h throughput (for 4-nm Al₂O₃) with specified non-uniformity <3%, uptime of 98% and a breakage rate of <0.02%. Although most ALD systems have an inherent drawback of wrap-around deposition, the KF-series have been modified to allow for single-side deposition.⁸² This system has a low tri-methyl-aluminium (TMA) consumption (~1 mg/wafer) and operational costs of RMB 0.03 per wafer. This six-tube batch

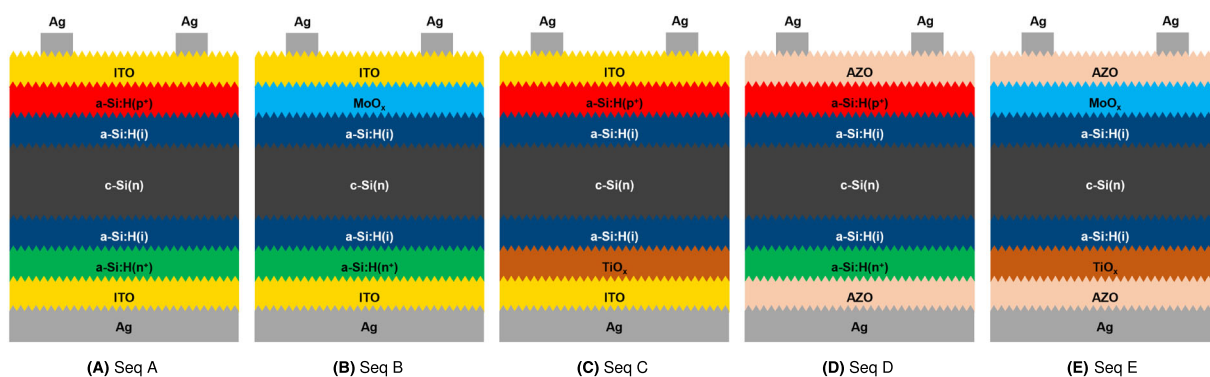


FIGURE 5 Schematics of the different solar cell structures analysed in this work. Seq A—standard HJT, Seq B—HJT with MoO_x, Seq C—HJT with TiO_x, Seq D—HJT with AZO and Seq E—HJT with all three ALD TMO layers

system can have maintenance on each tube independently to better suit high-volume manufacturing.

A key factor for equipment running cost per wafer produced is the throughput of the equipment. Since the TMO layers we are evaluating are different from Al_2O_3 , it is necessary to adjust the throughput to match the new process. The KF20000S is a six-tube system with a capacity of 1000 wafers per tube. This implies that the 20,000 wafer/h for (Al_2O_3) is achieved using a batch time of 18 min. For the new TMO layers analysed here, the thicknesses, cycle times and the number of cycles may not be the same as for Al_2O_3 , so we estimate the processing time based on the number of ALD cycles and the cycle time (second per cycle) observed during process development on a laboratory ALD system (Cambridge Nanotech's Fiji G2). The assumed thickness of the MoO_x layer was 4 nm based on the record efficiency for this type of structure.²³ For TiO_x , a 3-nm layer was the optimized thickness.⁹⁷ For TiO_x , it may be possible to use a thinner layer, which would further reduce cost, as 1.5 nm has been used successfully.¹⁷ For AZO, a thickness of 75 nm was selected based on optimal anti-reflective properties.²⁸ These assumptions and calculated throughput are shown in Table 2, where the throughput for MoO_x and TiO_x are similar to that of Al_2O_3 . The throughput calculations for AZO were very different for two reasons: (i) the film is significantly thicker, requiring many more cycles, and (ii) the need for deposition on both sides of the wafer. Regarding the latter, since TCOs are needed on both sides of the HJT, we can choose to complete two single-sided depositions or one double-sided deposition. A double-side deposition of AZO is possible in this ALD tool by modifying the wafer loading—the batch size is reduced by one third based on advice from the equipment manufacturer, ensuring sufficient space between the wafers and uniform precursor coverage. Despite the smaller batch size, this is the lowest-cost approach, since both the front and rear sides are deposited simultaneously. These throughput estimates are subject to uncertainty, for example, it may be that a lower or higher purge time is needed per cycle once each process is optimized for industrial scale and throughput. On the negative side, there are risks that scaling up

the lab process to an industrial scale will require longer process times to achieve good uniformity or properly purge the chamber. On the positive side, there may be a way to more densely load the chamber. Overall, we anticipate that the likelihood of faster throughput is lower than the likelihood of slower throughput, and so we use an uncertainty range in the wafer throughput (wafer/h) of +10%/–20% in the cost model.

Other input parameters used were based on the data sheets with uncertainty ranges applied. These are shown in Table 3. For those parameters where information was not readily available, our own estimate with wide uncertainty range was applied. This was done in line with the methodology—if wide uncertainty ranges on certain variables do not introduce significant impact on the resulting cost analysis, then there is no need to further investigate and refine these variables until other uncertainties are reduced. In the supporting information, other factory assumptions are described in Table S6.

To calculate materials costs, we must determine the most appropriate precursors to use and then estimate the usage of the precursor in each ALD process. For MoO_x , we selected the most common Mo precursor bis(tert-butylimido)-bis(dimethylamido)molybdenum because of its capacity to be deposited under low processing temperatures and the flexibility of using ozone or oxygen plasma^{98–100} as co-reactants. For TiO_x , the most widely used Ti precursors are TiCl_4 ,¹⁹ titanium isopropoxide,¹⁰¹ and tetrakis(dimethylamino)titanium (TDMAT), while water¹⁰² or ozone¹⁰³ are used as the oxidant. In our experiments and for the cost modelling, we assume the use of TDMAT, which produces non-corrosive and non-toxic by-products,¹⁰⁴ which is environmentally friendly and safe for industrial use. For AZO, we selected DEZ and TMA as they are the most common Zn and Al precursors, respectively.^{78,93,105} Regarding precursor usage, while the ALD process can in theory be carried out with nearly 100% precursor utilization, if exactly the correct amount of precursor is released into the chamber, practical considerations such as over-filling the chamber to decrease processing time, less reactive precursors, lower sticking probability, slow nucleation rate and deposition on chamber walls would result in lower utilization.

TABLE 2 Throughput assumptions for Monte Carlo analysis of ALD deposition costs

	MoO_x	TiO_x	AZO	Comment
Batch size (wafers)	6000	6000	4000	For AZO, the double-sided deposition means fewer wafers are loaded each batch.
Deposition thickness (nm)	4	3	75	–
Deposition cycles	36	66	480	Number of cycles based on experimental experience, includes some nucleation cycles.
Average thickness deposited per cycle (nm)	0.111	0.045	0.156	Note: after nucleation, growth rate is higher than this.
Cycle time (s)	30.1	30.1	20.1	Includes pulse 1st + purge + pulse 2nd + purge
Total process time per batch (minutes)	18.1	33.1	161	–
Throughput (wafer/h)	19,934	10,873	1493	–
Low throughput	15947	8698	1194	20% lower throughput is possible if process cannot be optimized for speed
High throughput	21,927	11,960	1642	10% higher throughput is possible if the wafer load size could be improved, or cycle time reduced

TABLE 3 Other equipment assumptions

	Mid value	Low	High	Comment
Tool cost (US\$ million)	1.8	1.44	1.98	List price was RMB 12 million. Converted using 0.15 USD per RMB. +10% / -20%
Facilities capital cost (% of tool cost)	20	10	25	
Maintenance (%)	1.5	1	2	Specification of uptime >98%
Equipment floorspace (m ²)	80	70	90	
Electrical power (kW)	100	90	110	Specification is 100 kW
Maintenance spare parts (% of capex per year)	3.5	2	5	
Operators per tool	0.3	0.1	0.5	System is fully automated, but some operators for loading and monitoring assumed
Maintenance personnel per tool	3	2	4	
Oxygen flow (standard lpm)	20	10	50	For ozone generation—per tool
Nitrogen flow (standard lpm)—pump purge	240	240	240	Per tool
Nitrogen usage (standard litres)—load lock vent	3500	3500	3500	Per tube vent

Note: Author estimates from data sheets and personal communication, with uncertainty ranges added to account for possible variations.

TABLE 4 Data on precursor usage

	MoO _x (1:2.9)	TiO _x	ZnO (bifacial AZO)	Al ₂ O ₃ (bifacial AZO)	Comment/Source
Thickness (nm)	4	3	142.5	7.5	See text
Wafer area (cm ² /wafer)	252	252	252	252	M3 wafer
Volume of layer (cm ³ /wafer)	0.00010	0.00008	0.00359	0.00019	Calculated
Density of layer (g/cm ³)	4.0	4.23	5.6	3.987	104,106,107
Mass of layer (g/wafer)	0.00040	0.00032	0.0201	0.00075	Calculated
Molar mass of layer (g/mol)	142.8	79.9	81.4	101.9	Data sheets
Moles of layer (mol/wafer)	2.82E-06	4.00E-06	0.000247	7.39E-06	Calculated
Precursor name	(tBuN) ₂ (NMe) ₂ Mo	TDMAT	DEZ	TMA	
Molar mass of precursor (g/mol)	326.33	224.00	123.00	144.20	Calculated
Ratio of moles of precursor to moles of layer	1	1	1	2	
Mass of precursor (100% utilization) g/wafer	0.00092	0.00090	0.0304	0.00213	Calculated
Mid usage (g/wafer)—80% material utilization	0.00115	0.00112	0.0380	0.00266	Calculated
Low usage (g/wafer)—90% material utilization	0.00102	0.00100	0.0338	0.00237	Calculated
High usage (g/wafer)—70% material utilization	0.00132	0.00128	0.0434	0.00304	Calculated

In a lab environment, utilization rates close to 50% have been reported,⁸⁶ but for industrial ALD use,⁸² very high utilization of precursors have been claimed for Al₂O₃ (1 mg/wafer of TMA for 4 nm is close to 100% utilization). The actual utilization rate of precursors is a significant unknown that is best determined by demonstrating an optimized process in industrial-sized equipment. To account for this uncertainty, we base our range of precursor usage on utilization between 70% and 90%. A wafer area of 252 cm² (G1) was assumed to match with the NREL 2021 HJT cost analysis. The assumptions and calculations for precursor usage are shown in Table 4.

The cost of ALD precursors in a research setting is very high since a relatively small amount of precursor (typically 25 g) is purchased at one time. One of the ALD precursors (TMA) is currently used in industrial quantities. For lab quantities (25 g), research institutes pay

around US\$ 100 /g. In 2016, one report estimated TMA costs at EUR 0.75/g,¹⁰⁸ and industry contacts of the authors suggested that at manufacturing volumes, it is currently possible to purchase this for \$ 0.2/g. This is an extraordinarily large cost reduction. Part of the reason for this low cost is that lower cost 'solar grade TMA' can be used instead of semiconductor grade,¹⁰⁵ a cost reduction of 10 times. Other factors are presumably the advantage of economies of scale in manufacturing, handling and transporting the pyrophoric precursor.

For the other precursors, firm large volume pricing information was not available. Making use of the Monte Carlo uncertainty approach, we estimated a range of possible costs for each precursor to understand our sensitivity to this factor. Two approaches were considered for estimating the possible range of the cost of precursors in large volumes. The first option was to assume the cost reduction

between lab and industry pricing for TMA would be repeated for other precursors—a roughly 500 times cost reduction. This is an optimistic approach, and it assumes that a lower purity ‘solar grade’ precursor could similarly be used, and that the same drivers for economies of scale are available. Instead, we use a more conservative approach, described in other work,¹⁰⁹ and use an economies of scale model to estimate high-volume pricing based on low volume pricing. As in previous work, an uncertainty range of the ‘doubling factor’ (the cost multiplier for every doubling of purchase volume) can be used to identify a range of high-volume prices. In this work, a production volume of 210 million solar cells per year (~ 1 GW/yr) is assumed, and the extrapolated price range using this method is also shown in Table 5. The range of possible doubling factors was varied between a low of 0.75 and a high of 0.95. This resulted in a cost reduction range between 3 and 30 times. This range was cross checked with indicative pricing (100kg/year, ex works) from a supplier—TDMAT at \$5/g was close to the mid value, and DEZ at \$0.8/g was between the mid and high value. No volume cost information was available for the Mo precursor used in our lab. Because there are still many unknowns to these costs, such as required purity, shipping and packaging, we kept the large uncertainty range within the Monte Carlo model to check sensitivity to this pricing, and this is discussed further in the sections below.

The other materials used in ALD are nitrogen (for pump purging and chamber venting) and oxygen (to generate ozone as the oxygen

source). In experimental work, DI water (negligible cost) was used as the oxygen source; however, advice from industry was that ozone-based processes are preferred in production due to reduced purge times and improved uniformity. Nitrogen and oxygen usage per solar cell are calculated based on estimated flow (Table 3) and equipment throughput.

4.3 | Results for ALD TMO deposition

Once these input data were used in the Monte Carlo cost model, the cost distributions shown in Figure S5 were obtained. A cost breakdown is shown in Figure 6, where each process is compared to the process(es) that they are partially or completely replacing. For the MoO_x and TiO_x layers, they are replacing half of the corresponding PECVD layers (the doped a-Si layers). For the AZO double-sided layers, they are replacing the entire front and rear sputtered ITO layers.

An analysis of variance was completed for each of the layers to determine the input parameters to the cost model that contributed most to this uncertainty, with the results shown in Figure 7.

For the hole (MoO_x) layer (Figure 6A), the cost is dominated by materials, with a very large uncertainty. The median of the cost estimate is 1.6 c/cell, 10th percentile 0.7 c/cell and 90th percentile 5 c/

TABLE 5 Data on precursor costs at manufacturing scale

Precursor Name	Mo	TDMAT	DEZ	TMA
Lab purchase amount (g)	25	25	2000	
Lab purchase cost (US\$/g)	76.4	33.5	2.2	
Annual usage (wafers/year)	210,000,000	210,000,000	210,000,000	
Mid estimate usage (g/wafer)	0.00115	0.00112	0.0380	
Annual precursor usage (g/year)	241,868	235,338	7,976,520	
Number of doublings of purchase quantity	13.2	13.2	12.0	
Mid projected cost (0.85 doubling factor) US\$/g	8.9	3.9	0.31	0.20
Low projected cost (0.75 doubling factor) US\$/g	1.7	0.75	0.07	0.15
High projected cost (0.95 doubling factor) US\$/g	39	17	1.2	0.3

Note: For TMA, industrial scale cost data are available, so the economies of scale model is not used.

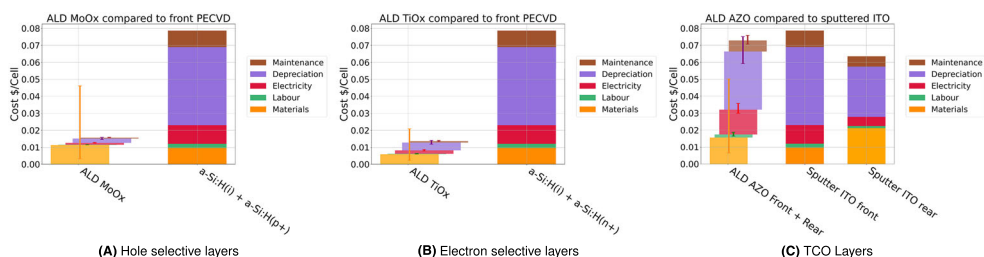


FIGURE 6 Cost breakdown for ALD TMO layer alternatives. Panel (A) shows the cost of the MoO_x layer compared to the front PECVD a-Si:H layers, (B) shows the cost of the TiO_x layer compared to the rear PECVD a-Si:H layers and (C) shows the double-sided ALD AZO layer cost compared to the front and rear Sputter ITO layers it replaces. For each cost component, the height of the bar is the median value, and the error bar shows the 10th and 90th percentile values of that cost component to indicate the uncertainty. The cost components are offset to allow easier viewing of the error bars

cell (Figure S5a). The cost of the doped a-Si:H layer this replaces is 2.1 c/W, so there is no guarantee that the ALD MoO_x layer will reduce the cost in \$/cell. The large uncertainty is primarily due to not knowing the cost of purchasing very large quantities of the precursor and is also impacted by uncertainty in the precursor utilization rate. The impact of these two parameters on the layer cost can be seen graphically in Figure S5d, where every iteration of the Monte Carlo analysis is plotted against these two parameters, and the total cost of the layer is shown in the colour scale. A fit to these data is shown in Figure 7A. From these figures, we can see that precursor costs of around \$20/g (compared to \$75/g in lab quantities) could lead to layer total costs between 2.4 and 3.2 c/cell, depending on the precursor usage per wafer.

For the electron (TiO_x) layer (Figure 6B), the cost and uncertainty are much lower than for MoO_x, with the 10th, 50th and 90th percentile cost 1.0, 1.4 and 2.9 c/cell, respectively (Figure S5b). The materials cost is similar to the equipment depreciation; however, there is more uncertainty contributed from materials costs. In this case, the precursor cost uncertainty is the main source of variance, followed by the throughput uncertainty of the ALD equipment. The relationship between these two variables and the layer cost are shown in Figure 7B (with the Monte Carlo points shown in Figure S5e).

For both the MoO_x and TiO_x layers, the depreciation and maintenance costs are remarkably low compared to the PECVD process they are partially replacing. The reason for this is the relative capital cost and throughput of the respective equipment. For MoO_x, for example, the equipment cost of around US\$ 1.8 M, and a throughput of nearly 20k wafer/h means such a tool can process more than 800 MW/year, a capital cost of approx. 0.0023 US\$ per W of annual capacity (US\$/W_{cap}). In comparison, the PECVD data in the NREL database have a toolset capital cost of approximately US\$0.040/W_{cap}. The depreciation value per produced watt can be calculated by dividing over the depreciation period (5 years). Maintenance labour costs are relatively low due to the high up-time (98%), and maintenance spare parts costs are very low based on advice from the manufacturer.

For the AZO (Figure 6C), the median total cost of 7.6 c/cell is attractive compared to the cost of the front and rear ITO layers (total cost 10.4 c/cell). However, there is significant uncertainty in both the materials and depreciation costs (Figure S5c), and the 90th percentile value of the cost estimate (11.1 c/cell) is more expensive than the ITO layers. In comparison to the hole and electron layers, AZO layer is much more expensive. This is because of the double-

sided deposition of a much thicker layer (75 nm). This requires many more ALD cycles, which reduces the equipment throughput and therefore increases the equipment depreciation cost. The usage of precursors is also much higher because of the thicker layer, but this is somewhat mitigated by the comparatively low cost of the zinc precursor that makes up most of the layer. It is uncertainty in the cost of the zinc precursor that is most critical, followed by the uncertainty of the equipment throughput. The relationship between these variables and the layer cost are shown in Figure 7C (Monte Carlo iterations shown in Figure S5f).

4.4 | Cost comparisons of solar cell sequences

We now consider the impact of incorporating these TMO layers into different solar cell fabrication sequences. We define sequences as shown in Table S5, and images of each are shown in Figure 5.

The cost of each of these sequences is shown as a step-by-step breakdown in Figure S6. The cost of standard HJT processes were taken from the NREL data but converted from \$/W to \$/cell to allow the calculation of cost independent of efficiency. One important factor in this analysis is the cost of the a-Si deposition and how much this will reduce if the doped a-Si layer is not required. The NREL cost data combine the cost of the intrinsic and doped a-Si double layer into one process, since these layers are deposited sequentially within the same tool without breaking vacuum. However, for the analysis of the ALD TMO processes, we need to deposit the intrinsic a-Si layer only. Since the thickness of the intrinsic and doped a-Si layers are similar, and have similar deposition rates, avoiding the doped layer deposition will roughly halve the processing cost. However, since wafer loading and unloading times will not change, we assume that only 40% of the cost is saved.

4.4.1 | Sequence B—HJT with ALD molybdenum oxide

As seen comparing Figure S6b to Figure S6a, the cost of the MoO_x layer could be lower than the cost of the p-type a-Si layer, thus providing a cost benefit in \$/cell. This potential cost advantage needs to be balanced against any possible solar cell performance difference, which can be done by examining the Monte Carlo uncertainty model data, combined with an exploration of the impact of an efficiency

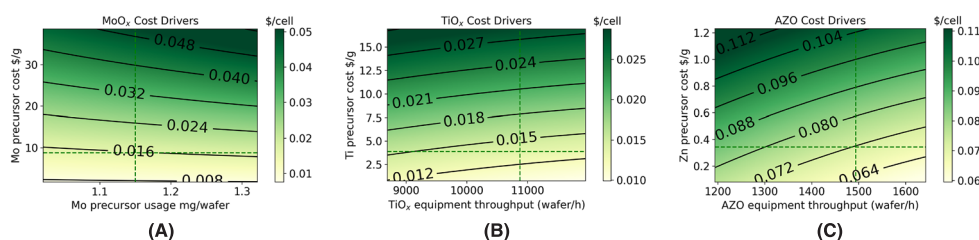


FIGURE 7 Key cost drivers and their impact on total layer deposition cost for ALD deposition of (A) MoO_x, (B) TiO_x and (C) AZO. These are fits to the Monte Carlo data shown in Figure S5d–f

deficit or improvement. Figure 8 shows the conditions where the MoO_x sequence has improved (blue) or worse (red) cost performance in solar cell \$/W. If the projected cost of the MoO_x layer is at the upper end of our estimate (5 c/cell), and if there was no efficiency difference to HJT, then the MoO_x sequence would be approximately 0.5 c/W more expensive. However, if the cost of MoO_x were lower, at approximately 1 c/cell, then at equal efficiency, the cost would be around 0.2 c/W cheaper. The zero-contour line indicates the break-even region of cost and efficiency and can be used to identify a target efficiency difference between this structure and standard HJT. For example, even if the layer can be deposited at the lower cost of 1 c/cell, the efficiency of this structure can be at worst 0.2%_{abs} lower than standard HJT.

As shown in Figure 2, the best lab demonstration of Seq B has an efficiency of 23.5%, which in that experiment was a similar value to that obtained with the standard HJT control solar cells.²³ Although very promising, when compared to the best lab non-IBC HJT efficiency of 26.3%,⁶ this is still 2.8%_{abs} lower, a deficit that is too large for this sequence to be cost-competitive. Further work is needed to improve the best lab efficiency beyond 26%, which is not impossible since the fundamental efficiency limit imposed by MoO_x is 26.9%,⁴ and since it also offers the advantage of significantly lower parasitic absorption when applied to the front of the solar cell.

Even if the efficiency of this MoO_x structure can match standard HJT cells, it is necessary for the cost of processing the MoO_x layer to be less than 2 c/cell in order to obtain an advantage in \$/W. This presents an important area of research that should be carried out in parallel to efficiency improvements. From Figure 7A, we see that 2 c/cell requires a Mo precursor cost of between 10 and 15 \$/g, depending on the precursor usage per wafer. Researchers should therefore seek to optimize and demonstrate high utilization of precursors. It is also important to investigate the cost of this MoO_x precursor at manufacturing volumes. If there are indications that this precursor will

be too expensive, alternative Mo precursors will need to be identified and tested for their performance.

In review, the cost analysis indicates that further research is needed to improve efficiency towards its full potential in order to realise the cost benefits of MoO_x.

4.4.2 | Sequence C—HJT with ALD titanium dioxide

In a similar way, comparing Figure S6c to Figure S6a, the median cost of the TiO_x layer is lower than the cost of the n-type a-Si layer. The trade-off in cost and efficiency is shown in Figure 9. If we consider the best case from a cost perspective—if the TiO_x process is around \$ 0.01/cell—then the efficiency of this sequence needs to be at worst 0.2%_{abs} lower than that of standard HJT to be cost competitive.

Currently this sequence, a TiO_x/i-a-Si:H stack in combination with ITO as electron contact, is yet to be demonstrated experimentally, but a similar structure using SiO₂ as the passivation layer together with TiO_x as the electron selective contact has achieved 22.1%.⁵¹ This is 4.2%_{abs} lower than the best non-IBC HJT solar cell,⁶ so for this technology to have a chance of being competitive, it is necessary to match and then exceed this efficiency significantly. The fundamental efficiency limit imposed by a passivating contact with TiO_x is well over 27%,⁴ indicating that efficiency parity with standard HJT solar cells is feasible with additional development resources.

If this efficiency gap can be bridged in the lab, then the cost uncertainty and its impact on economic competitiveness is relevant. Cost related research should focus on precursor costs, and also ensure high throughput by keeping the ALD cycle time short. Another pathway to keeping the cost of this layer low is to demonstrate high efficiency with the use of a thinner TiO_x layer—such as the 1.5 nm used by Bullock et al¹⁷ instead of the assumed 3 nm here.

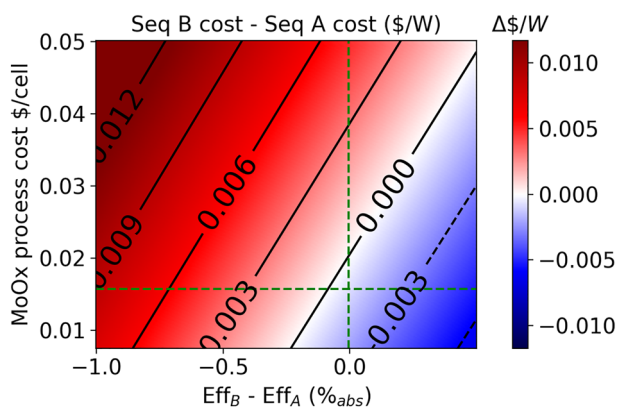


FIGURE 8 Comparison between Seq A (Figure 5A, standard HJT) and Seq B (Figure 5B HJT but using MoO_x instead of p-doped a-Si). Fit to data from the Monte Carlo analysis (Figure S5g), showing the impact of layer cost and efficiency difference on the difference in cost between the sequences, where blue indicates Seq B is lower cost (\$/W)

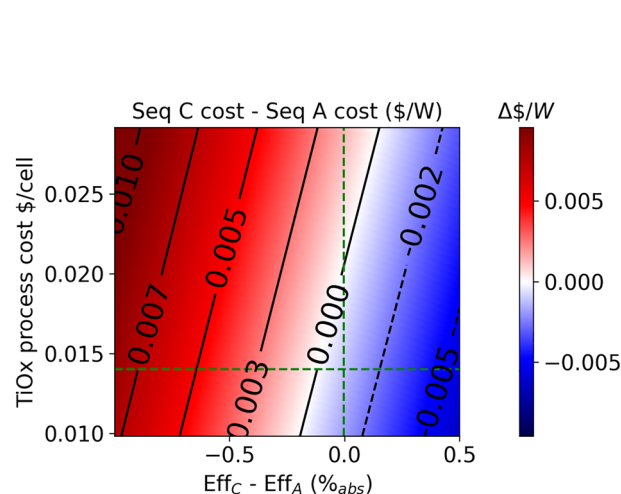


FIGURE 9 Fit to data from the Monte Carlo analysis (Figure S5h) showing the impact of key drivers on the difference in \$/W of using TiO_x to replace n-doped a-Si

4.4.3 | Seq D—HJT with ALD aluminium-doped zinc oxide

Similarly, comparing Figure S6d to Figure S6a, the cost of the AZO layers is expected to be comparable to the cost of depositing one of the ITO layers. Since the AZO cost includes depositing both sides simultaneously, the total cost of both front and back ITO is compared with AZO. The trade-off in cost and efficiency is seen in Figure 10. Depending on the eventual cost of the AZO process, the new process could be competitive even if it results in lower performance. For example, if the AZO layer costs 8 c/cell (near the median of the cost estimate), the structure could be 0.4% lower efficiency and still achieve cost parity. If the AZO layer is 6 c/cell (the lower end of the estimate), and the efficiency could be the same as standard HJT, this would save approx 0.7 c/W.

Considering the potential efficiency of this sequence, as outlined in Section 3.1, replacing ITO with ALD AZO can result in efficiency parity to standard HJT solar cells. At efficiency parity, the AZO replacement of ITO is cost effective as long as the AZO cost is less than 10 c/cell.

Another motivation for AZO as a replacement for ITO is that indium is an expensive metal with limited supply that has had increasing demand from products such as touch screens and flat panel

displays.¹¹⁰ If solar cell technologies such as HJT (that use ITO layers) increase in popularity, this will increase demand pressures. It is quite possible that supply and demand dynamics lead to a significant increase in indium prices in the future. Based on the cost data from NREL (Figure S4a,b), 50% of the ITO process cost is related to the materials, mostly comprising the ITO sputter target. As an indication of possible cost fluctuations, if ITO target costs were exactly proportional to the indium market price, then a 20% indium price increase would result in a 10% increase in the cost of the ITO process.

To explore the sensitivity of this result to ITO cost, we adapted the model to include a variation of ITO layer costs, as shown in Figure 11. If the total ITO layer cost was to increase 25% (ITO cost ratio 1.25, right), the cost benefit of AZO becomes even stronger. Conversely, if ITO deposition costs were to reduce by 25% (the left figure), AZO would still be cost competitive if it can have efficiency parity and the layer cost is less than 7.7 c/cell.

From this analysis, we see that ALD AZO has great potential as an ITO replacement, as it is likely lower cost than the ITO alternative and does not face the same cost pressure from indium shortages. This motivates further work to demonstrate it can achieve efficiency parity to ITO in an industrial setting.

4.4.4 | Seq E—Three ALD layers combined

Finally, we consider the possibility of combining all three of the proposed TMO layers into one structure. By using MoO_x , TiO_x and AZO together, there is the potential to reduce costs overall if a high efficiency can be achieved, as well as reduce sensitivity to indium prices. This comparison can be seen in Figure 12, which indicates that if the three ALD TMO processes are at the median value of their cost range, the sequence could be cost-competitive even with a 0.5%_{abs} efficiency deficit compared to standard HJT.

A solar cell that incorporates all three ALD TMO layers has not yet been experimentally demonstrated; however, as described in Section 3.1, the best laboratory efficiency that incorporates MoO_x (thermally evaporated, not ALD) and TiO_x (ALD) is 20.7%,¹⁷ 5.6%_{abs} lower than the best non-IBC HJT solar cell.⁶ The analysis of Schmidt et al⁴ calculates an efficiency limit of 26%, and any improvements developed for MoO_x -only or TiO_x -only sequences could potentially be combined into this more complex structure. The 20.7% result used

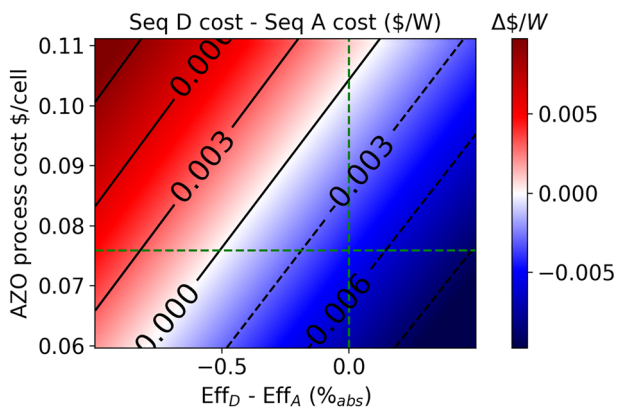


FIGURE 10 Fit to data from the Monte Carlo analysis (Figure S5i), showing the impact of key drivers on the difference in cost in \$/W of using AZO to replace ITO

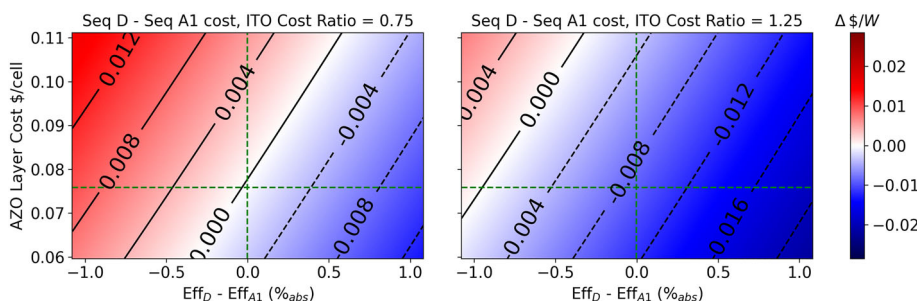


FIGURE 11 Comparison in \$/W of using AZO to replace ITO, but where a possible increase in ITO processing cost is explored

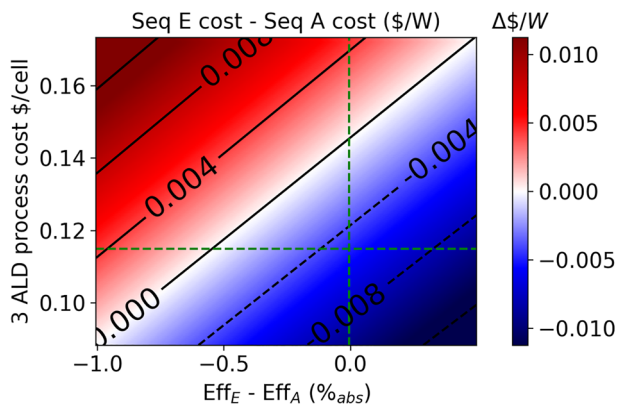


FIGURE 12 Fit to data from the Monte Carlo analysis showing the impact of the total ALD TMO process costs and efficiency difference on the difference in cost in \$/W of Seq E compared to standard HJT

ITO, not AZO, however as described in Section 3.1, many experiments are showing that ALD AZO can give efficiency parity to ITO, so a combination of all three ALD TMO layers has the potential to achieve similar efficiencies to standard HJT.

5 | CONCLUSIONS

We have built a cost model to help understand the cost drivers of TMO layers formed by ALD and assessed the cost and efficiency targets required for three alternative use cases in passivated contact solar cells. We found that these ALD deposited TMO layers have the potential to be lower cost (per cell) than the doped a-Si and ITO currently used in HJT solar cells. The key factors that determine the cost are slightly different for each ALD layer, but in all cases, the costs of the precursors at industrial volumes are the most important.

While lower production costs per cell may be achievable, this will not result in lower production costs in \$/W unless the resultant solar cell efficiency is high enough. The combined impact of solar cell efficiency and TMO layer costs on the relative cost in \$/W between the TMO sequences and standard HJT is shown for each of the alternatives considered. In exploring these relationships, we identify efficiency targets that must be met, even if the ALD TMO layers are at the lower end of our cost estimates. Efficiency limit analysis indicate that with further development, the proposed solar cell architectures using ALD TMO layers could reach efficiency parity with standard HJT. If this was achieved, then the architectures using AZO would be competitive in \$/W cost, even if the TMO layer costs are on the higher side of expectations. For the MoO_x and TiO_x architectures, achieving efficiency parity alone may not be sufficient, since high Mo and Ti precursor costs would lead to a more expensive process. This motivates investigations into alternate or lower purity precursors and firmer volume pricing. The use of AZO as a replacement TCO for ITO has particular merit if indium costs were to increase due to increased demand from the solar and other industries. In this work, we provide motivation and targets for continued work to demonstrate high solar

cell efficiency using TMO layers in parallel to clarifying industrial throughput and high-volume precursor costs.

ACKNOWLEDGEMENTS

This work has been supported by the Australian Government through the Australian Renewable Energy Agency (ARENA) as part of ARENA's Research and Development Program - Solar PV Research (Grant 2017/RND007) and the Australian Centre of Advanced Photovoltaics (ACAP). Open access publishing facilitated by University of New South Wales, as part of the Wiley - University of New South Wales agreement via the Council of Australian University Librarians. [Correction added on 18 May 2022, after first online publication: CAUL funding statement has been added.]

CONFLICTS OF INTEREST

There are no conflicts to declare.

DATA AVAILABILITY STATEMENT

The data that supports the findings of this study are available in the supplementary material of this article.

ORCID

Nathan L. Chang <https://orcid.org/0000-0003-2744-582X>

Mohammad Dehghanimadvar <https://orcid.org/0000-0001-8160-5455>

Renate J. Egan <https://orcid.org/0000-0002-8970-4703>

Bram Hoex <https://orcid.org/0000-0002-2723-5286>

REFERENCES

- International Technology Roadmap for Photovoltaic (ITRPV), 2020 results, 12th edition, SEMI; 2021.
- World Energy Investment 2021, IEA, Paris; 2021. <https://www.iea.org/reports/world-energy-investment-2021>
- China PV Industry Development Roadmap, 2020 edition, CPIA; 2020.
- Schmidt J, Peibst R, Brendel R. Surface passivation of crystalline silicon solar cells: present and future. *Sol Energy Mater Sol Cells*. 2018; 187:39-54.
- Longi sets record of 25.09% for n-type topcon cell efficiency. Longi Solar https://en.longi-solar.com/home/events/press_detail/id/335.html; 2021.
- Longi sets new world record of 25.82% for HJT solar cell efficiency. 2021.
- Masuko K, Shigematsu M, Hashiguchi T, et al. Achievement of more than 25% conversion efficiency with crystalline silicon heterojunction solar cell. *IEEE J Photovoltaics*. 2014;4(6):1433-1435.
- Terakawa A, Murayama H, Naruse Y, et al. Panasonic's thin film silicon technologies for advanced photovoltaics. *MRS Online Proc Libr (OPL)*. 2013;1536:17-26.
- Yoshikawa K, Yoshida W, Irie T, et al. Exceeding conversion efficiency of 26% by heterojunction interdigitated back contact solar cell with thin film si technology. *Sol Energy Mater Sol Cells*. 2017;173:37-42.
- Feldmann F, Bivour M, Reichel C, Hermle M, Glunz SW. Passivated rear contacts for high-efficiency n-type si solar cells providing high interface passivation quality and excellent transport characteristics. *Sol Energy Mater Sol Cells*. 2014;120:270-274.
- Feldmann F, Bivour M, Reichel C, Steinkemper H, Hermle M, Glunz SW. Tunnel oxide passivated contacts as an alternative to partial rear contacts. *Sol Energy Mater Sol Cells*. 2014;131:46-50.

12. Glunz SW, Feldmann F, Richter A, et al. The irresistible charm of a simple current flow pattern—25% with a solar cell featuring a full-area back contact. In: Proceedings of the 31st european photovoltaic solar energy conference and exhibition; 2015:259-263.
13. Moldovan A, Feldmann F, Kaufmann K, et al. Tunnel oxide passivated carrier-selective contacts based on ultra-thin SiO₂ layers grown by photo-oxidation or wet-chemical oxidation in ozonized water. In: 2015 IEEE 42nd Photovoltaic Specialist Conference (PVSC) IEEE; 2015:1-6.
14. Richter A, Benick J, Feldmann F, Fell A, Hermle M, Glunz SW. n-Type si solar cells with passivating electron contact: identifying sources for efficiency limitations by wafer thickness and resistivity variation. *Sol Energy Mater Sol Cells*. 2017;173:96-105.
15. Richter A, Müller R, Benick J, et al. Design rules for high-efficiency both-sides-contacted silicon solar cells with balanced charge carrier transport and recombination losses. *Nat Energy*. 2021;6(4):429-438.
16. Haase F, Hollemann C, Schäfer S, et al. Laser contact openings for local poly-Si-metal contacts enabling 26.1%-efficient polo-ibc solar cells. *Sol Energy Mater Sol Cells*. 2018;186:184-193.
17. Bullock J, Wan Y, Xu Z, et al. Stable dopant-free asymmetric heterocontact silicon solar cells with efficiencies above 20%. *ACS Energy Lett*. 2018;3(3):508-513. doi:10.1021/acseenergylett.7b01279
18. Lin W, Boccard M, Zhong S, et al. Degradation mechanism and stability improvement of dopant-free ZnO/LiF/x/Al electron nanocontacts in silicon heterojunction solar cells. *ACS Appl Nano Mater*. 2020;3(11):11391-11398. doi:10.1021/acsnm.0c02475
19. Yang X, Bi Q, Ali H, Davis K, Schoenfeld WV, Weber K. High-performance TiO₂-based electron-selective contacts for crystalline silicon solar cells. *Adv Mater*. 2016;28(28):5891-5897.
20. Yang X, Zheng P, Bi Q, Weber K. Silicon heterojunction solar cells with electron selective TiOx contact. *Sol Energy Mater Sol Cells*. 2016;150:32-38.
21. Battaglia C, De Nicolas SM, De Wolf S, Yin X, Zheng M, Ballif C, Javey A. Silicon heterojunction solar cell with passivated hole selective moox contact. *Appl Phys Lett*. 2014;104(11):113902.
22. Battaglia C, Yin X, Zheng M, et al. Hole selective moo x contact for silicon solar cells. *Nano Lett*. 2014;14(2):967-971.
23. Dréon J, Jeangros Q, Cattin J, Haschke J, Antognini L, Ballif C, Boccard M. 23.5%-efficient silicon heterojunction silicon solar cell using molybdenum oxide as hole-selective contact. *Nano Energy*. 2020;70:104495.
24. Geissbühler J, Werner J, Martin de Nicolas S, et al. 22.5% efficient silicon heterojunction solar cell with molybdenum oxide hole collector. *Appl Phys Lett*. 2015;107(8):081601.
25. Woodhouse MA, Smith B, Ramdas A, Margolis RM. Crystalline silicon photovoltaic module manufacturing costs and sustainable pricing: 1H 2018 benchmark and cost reduction road map, Golden, CO (United States), National Renewable Energy Lab.(NREL); 2019.
26. Solar cells and module technology trends analysis, 2021, Infolink Consulting Group; 2021.
27. Brendel R, Peibst R. Contact selectivity and efficiency in crystalline silicon photovoltaics. *IEEE J Photovoltaics*. 2016;6(6):1413-1420.
28. Holman ZC, Descoeurdes A, Barraud L, et al. Current losses at the front of silicon heterojunction solar cells. *IEEE J Photovoltaics*. 2012; 2(1):7-15.
29. Meyer J, Hamwi S, Kröger M, Kowalsky W, Riedl T, Kahn A. Transition metal oxides for organic electronics: energetics, device physics and applications. *Adv Mater*. 2012;24(40):5408-5427.
30. Liao B, Hoex B, Aberle AG, Chi D, Bhatia CS. Excellent C-Si surface passivation by low-temperature atomic layer deposited titanium oxide. *Appl Phys Lett*. 2014;104(25):253903. doi:10.1063/1.4885096
31. Thomson AF, McIntosh KR. Light-enhanced surface passivation of TiO₂-coated silicon. *Prog Photovolt Res Appl*. 2012;20(3):343-349. doi:10.1002/pip.1132
32. Cho J, Melskens J, Debucquoy M, et al. Passivating electron-selective contacts for silicon solar cells based on an a-si: H/TiOx stack and a low work function metal. *Prog Photovolt Res Appl*. 2018; 26(10):835-845.
33. Cho J, Melskens J, Payo MR, et al. Performance and thermal stability of an a-Si: H/tio x/yb stack as an electron-selective contact in silicon heterojunction solar cells. *ACS Appl Energy Mater*. 2019;2(2): 1393-1404.
34. Matsui T, Bivour M, Ndione P, Hettich P, Hermle M. Investigation of atomic-layer-deposited TiOx as selective electron and hole contacts to crystalline silicon. *Energy Procedia*. 2017;124:628-634.
35. Daineka D, Bulkin P, Girard G, Bourée J-E, Drévilion B. High density plasma enhanced chemical vapor deposition of optical thin films. *Eur Phys J-Appl Phys*. 2004;26(1):3-9.
36. Fujimura N, Ohta A, Makihara K, Miyazaki S. Evaluation of valence band top and electron affinity of SiO₂ and Si-based semiconductors using X-ray photoelectron spectroscopy. *Jpn J Appl Phys*. 2016; 55(8S2):08PC06.
37. Bedia FZ, Bedia A, Benyoucef B, et al. Electrical properties of ZnO/p-Si heterojunction for solar cell application. *Int J Mater Eng*. 2013; 3(4):59-65.
38. Wang W, He J, Yan D, et al. 21.3%-efficient n-type silicon solar cell with a full area rear TiOx/lif/al electron-selective contact. *Sol Energy Mater Sol Cells*. 2020;206:110291.
39. Macco B, Bivour M, Deijkers JH, et al. Effective passivation of silicon surfaces by ultrathin atomic-layer deposited niobium oxide. *Appl Phys Lett*. 2018;112(24):242105.
40. Wan Y, Karuturi SK, Samundsett C, et al. Tantalum oxide electron-selective heterocontacts for silicon photovoltaics and photoelectrochemical water reduction. *ACS Energy Lett*. 2017;3(1): 125-131.
41. Mews M, Lemaire A, Korte L. Sputtered tungsten oxide as hole contact for silicon heterojunction solar cells. *IEEE J Photovoltaics*. 2017; 7(5):1209-1215.
42. Yang X, Xu H, Liu W, et al. Atomic layer deposition of vanadium oxide as hole-selective contact for crystalline silicon solar cells. *Adv Electron Mater*. 2020;6(8):2000467.
43. Lin W, Wu W, Liu Z, et al. Chromium trioxide hole-selective heterocontacts for silicon solar cells. *ACS Appl Mater Interfaces*. 2018;10(16):13645-13651.
44. Maeng WJ, Choi D, Park J, Park JS. Atomic layer deposition of highly conductive indium oxide using a liquid precursor and water oxidant. *Ceram Int*. 2015;41(9):10782-10787.
45. Semma M, Gotoh K, Wilde M, Ogura S, Kurokawa Y, Fukutani K, Usami N. Impact of deposition of indium tin oxide double layers on hydrogenated amorphous silicon/crystalline silicon heterojunction. *AIP Adv*. 2020;10(6):065008. doi:10.1063/5.0009994
46. Li S, Shi Z, Tang Z, Li X. Comparison of ITO, In₂O₃:Zn and In₂O₃:H transparent conductive oxides as front electrodes for silicon heterojunction solar cell applications. *Vacuum*. 2017;145:262-267. <https://www.sciencedirect.com/science/article/pii/S0042207X17309521>
47. Igasaki Y, Ishikawa M, Shimaoka G. Some properties of Al-doped ZnO transparent conducting films prepared by RF reactive sputtering. *Appl Surf Sci*. 1988;33/34(C):926-933.
48. Selmane N, Cheknane A, Hilal HS. Optimization of Al-doped ZnO transparent conducting oxide and emitter layers for enhanced performance of Si heterojunction solar cells. *J Electron Mater*. 2020; 49(3):2179-2190. doi:10.1007/s11664-019-07917-w
49. Gatz HA, Koushik D, Rath JK, Kessels WMM, Schropp REI. Atomic layer deposited ZnO:B as transparent conductive oxide for increased short circuit current density in silicon heterojunction solar cells. *Energy procedia*, Vol. 92: Elsevier Ltd; 2016:624-632.
50. Potter DB, Bhachu DS, Powell MJ, Darr JA, Parkin IP, Carmalt CJ. Al-, Ga-, and In-doped ZnO thin films via aerosol assisted CVD for

- use as transparent conducting oxides. *Phys Status Solidi (A) Appl Mater Sci*. 2016;213(5):1346-1352. doi:10.1002/pssa.201532996
51. Yang X, Weber K, Hameiri Z, De Wolf S. Industrially feasible, dopant-free, carrier-selective contacts for high-efficiency silicon solar cells. *Prog Photovolt Res Appl*. 2017;25(11):896-904.
 52. Kan Z, Wang Z, Firdaus Y, Babics M, Alshareef HN, Beaujuge PM. Atomic-layer-deposited AZO outperforms ITO in high-efficiency polymer solar cells. *J Mater Chem A*. 2018;6(22):10176-10183. <https://pubs.rsc.org/en/content/articlehtml/2018/ta/c8ta02841a>
 53. Kim SM, Rim YS, Keum MJ, Kim KH. Study on the electrical and optical properties of ITO and AZO thin film by oxygen gas flow rate. *J Electroceram*. 2009;23(2-4):341-345. doi:10.1007/s10832-008-9452-z
 54. Minami T. Transparent conducting oxide semiconductors for transparent electrodes. *Semicond Sci Technol*. 2005;20(4):S35. doi:10.1088/0268-1242/20/4/004/meta
 55. Ghahfarokhi OM, Chakanga K, Geissendoerfer S, Sergeev O, Maydell K, Agert C. DC-sputtered ZnO:Al as transparent conductive oxide for silicon heterojunction solar cells with $\mu\text{c-Si:H}$ emitter. *Prog Photovolt Res Appl*. 2015;23(10):1340-1352. doi:10.1002/ppp.2570
 56. Meza D, Cruz A, Morales-Vilches AB, Korte L, Stannowski B. Aluminum-doped zinc oxide as front electrode for rear emitter silicon heterojunction solar cells with high efficiency. *Appl Sci*. 2019;9(5):862. <https://www.mdpi.com/2076-3417/9/5/862/htm>
 57. Morales-Vilches AB, Cruz A, Pingel S, et al. ITO-free silicon heterojunction solar cells with ZnO:Al/SiO₂ front electrodes reaching a conversion efficiency of 23%. *IEEE J Photovoltaics*. 2019;9(1):34-39. <https://ieeexplore.ieee.org/document/8493365/>
 58. Cruz A, Wang EC, Morales-Vilches AB, Meza D, Neubert S, Szyszka B, Schlatmann R, Stannowski B. Effect of front TCO on the performance of rear-junction silicon heterojunction solar cells: insights from simulations and experiments. *Sol Energy Mater Sol Cells*. 2019;195:339-345.
 59. Niemelä JP, Macco B, Barraud L, et al. Rear-emitter silicon heterojunction solar cells with atomic layer deposited ZnO:Al serving as an alternative transparent conducting oxide to In₂O₃:Sn. *Sol Energy Mater Sol Cells*. 2019;200:109953.
 60. Allen TG, Bullock J, Yang X, Javey A, De Wolf S. Passivating contacts for crystalline silicon solar cells. *Nature Energy*. 2019;4(11):914-928. <https://www.nature.com/articles/s41560-019-0463-6>
 61. Boccard M, Yang X, Weber K, Holman ZC. Passivation and carrier selectivity of TiO₂ contacts combined with different passivation layers and electrodes for silicon solar cells. In: Conference Record of the IEEE Photovoltaic Specialists Conference; 2016:2403-2407.
 62. Cuevas A, Wan Y, Yan D, et al. Carrier population control and surface passivation in solar cells. *Sol Energy Mater Sol Cells*. 2018;184:38-47.
 63. Haschke J, Dupré O, Boccard M, Ballif C. Silicon heterojunction solar cells: recent technological development and practical aspects—from lab to industry. *Sol Energy Mater Sol Cells*. 2018;187:140-153.
 64. Vijayan RA, Masilamani S, Kailasam S, Shivam K, Deenadhayalan B, Varadharajaperumal M. Study of surface passivation and charge transport barriers in DASH solar cell. *IEEE J Photovoltaics*. 2019;9(5):1208-1216.
 65. Wang Z, Li P, Liu Z, et al. Hole selective materials and device structures of heterojunction solar cells: recent assessment and future trends. *APL Mater*. 2019;7(11):110701. doi:10.1063/1.5121327
 66. Yang Z, Lin H, Sheng J, et al. Design principles of silicon heterojunction solar cells with dopant-free interdigitated back contacts. *Solar RRL*. 2019;3(11):1900230. doi:10.1002/solr.201900230
 67. Yu C, Xu S, Yao J, Han S. Recent advances in and new perspectives on crystalline silicon solar cells with carrier-selective passivation contacts. *Cryst*. 2018;8(11):430. <https://www.mdpi.com/2073-4352/8/11/430/htm>
 68. Zhong S, Morales-Masis M, Mews M, et al. Exploring co-sputtering of ZnO:Al and SiO₂ for efficient electron-selective contacts on silicon solar cells. *Sol Energy Mater Sol Cells*. 2019;194:67-73.
 69. Bilal B, Najeeb-ud Din H. Fundamentals of and recent advances in carrier selective passivating contacts for silicon solar cells. *J Electron Mater*. 2021;50(7):3761-3772. doi:10.1007/s11664-021-08933-5
 70. Lin W, Dréon J, Zhong S, et al. Dopant-free bifacial silicon solar cells. *Solar RRL*. 2021;5(5):2000771. doi:10.1002/solr.202000771
 71. Lee S, Cho I-S, Lee JH, et al. Two-step sol-gel method-based TiO₂ nanoparticles with uniform morphology and size for efficient photoenergy conversion devices. *Chem Mater*. 2010;22(6):1958-1965.
 72. Sun Y, Seo JH, Takacs CJ, Seifert J, Heeger AJ. Inverted polymer solar cells integrated with a low-temperature-annealed sol-gel-derived ZnO film as an electron transport layer. *Adv Mater*. 2011;23(14):1679-1683.
 73. Bullock J, Cuevas A, Allen T, Battaglia C. Molybdenum oxide MoO_x: a versatile hole contact for silicon solar cells. *Appl Phys Lett*. 2014;105(23):232109.
 74. Duerinckx F, Szlufcik J. Defect passivation of industrial multicrystalline solar cells based on PECVD silicon nitride. *Sol Energy Mater Sol Cells*. 2002;72(1-4):231-246.
 75. Heinemeyer F, Mader C, Münster D, Dullweber T, Harder N-P, Brendel R. Inline high-rate thermal evaporation of aluminum as a novel industrial solar cell metallization scheme. In: 2nd Workshop on Metallization for Crystalline Silicon Solar Cells; 2010.
 76. Johnson RW, Hultqvist A, Bent SF. A brief review of atomic layer deposition: from fundamentals to applications. *Mater Today*. 2014;17(5):236-246.
 77. Knez M, Nielsch K, Niinistö L. Synthesis and surface engineering of complex nanostructures by atomic layer deposition. *Adv Mater*. 2007;19(21):3425-3438.
 78. Puurunen RL. Surface chemistry of atomic layer deposition: a case study for the trimethylaluminum/water process. *J Appl Phys*. 2005;97(12):9.
 79. Hossain MA, Khoo KT, Cui X, et al. Atomic layer deposition enabling higher efficiency solar cells: a review. *Nano Mater Sci*. 2020;2(3):204-226.
 80. Schmidt J, Werner F, Veith B, et al. Industrially relevant Al₂O₃ deposition techniques for the surface passivation of si solar cells. In: Proceedings of the 25th European Photovoltaic Solar Energy conference; 2010; Valencia, Spain:1130-1133.
 81. French P, Krijnen G, Roozeboom F. Precision in harsh environments. *Microsyst Nanoengineering*. 2016;2(1):1-12.
 82. Schmela M. TAIYANG NEWS PERC Solar Cell Technology 2018 Edition; 2018.
 83. Metzler M, Patel R. Plasma enhanced chemical vapor deposition (PECVD) of silicon dioxide (SiO₂) using oxford instruments system 100 PECVD, University of Pennsylvania; 2017.
 84. Zhu G, Sun J, Guo X, Zou X, Zhang L, Gan Z. Numerical analysis of thickness uniformity of thin film deposited by rectangular planar target. In: 2017 18th International Conference on Electronic Packaging Technology (ICEPT) IEEE; 2017:1356-1360.
 85. Exarhos GJ, Zhou XD. Discovery-based design of transparent conducting oxide films. *Thin Solid Films*. 2007;515(18):7025-7052.
 86. Oviroh PO, Akbarzadeh R, Pan D, Coetzee RAM, Jen T-C. New development of atomic layer deposition: processes, methods and applications. *Sci Technol Adv Mater*. 2019;20(1):465-496.
 87. Asikainen T, Ritala M, Leskelä M, Prohaska T, Friedbacher G, Grasserbauer M. AFM and STM studies on In₂O₃ and ITO thin films deposited by atomic layer epitaxy. *Appl Surf Sci*. 1996;99(2):91-98.
 88. Lee D-J, Kwon J-Y, Lee JI, Kim K-B. Self-limiting film growth of transparent conducting In₂O₃ by atomic layer deposition using trimethylindium and water vapor. *J Phys Chem C*. 2011;115:15384-15389. <https://pubs.acs.org/sharingguidelines>
 89. Nilsen O, Balasundaraprabhu R, Monakhov EV, Muthukumarasamy N, Fjellvåg H, Svensson BG. Thin films of In₂O₃ by atomic layer deposition using In(acac)₃. *Thin Solid Films*. 2009;517(23):6320-6322.

90. Ott AW, Johnson JM, Klaus JW, George SM. Surface chemistry of In₂O₃ deposition using In(CH₃)₃ and H₂O in a binary reaction sequence. *Appl Surf Sci.* 1997;112:205-215.
91. Ritala M, Asikainen T, Leskelä M. Enhanced growth rate in atomic layer epitaxy of indium oxide and indium-tin oxide thin films. *Electrochem Solid-State Lett.* 1998;1(3):156-157.
92. Gao Z, Banerjee P. Review article: atomic layer deposition of doped ZnO films. *J Vac Sci Technol A.* 2019;37(5):050802. <http://creativecommons.org/licenses/by/4.0/>
93. Tynell T, Karppinen M. Atomic layer deposition of ZnO: a review. <http://stacks.iop.org/0268-1242/29/i=4/a=043001?key=crossref.8dff631b121191e73e94fde260e59441>; 2014.
94. Iqbal J, Jilani A, Ziaul Hassan PM, Rafique S, Jafer R, Alghamdi AA. ALD grown nanostructured ZnO thin films: effect of substrate temperature on thickness and energy band gap. *J King Saud Univ - Sci.* 2016;28(4):347-354. <https://www.sciencedirect.com/science/article/pii/S1018364715301105>
95. Yamada A, Sang B, Konagai M. Atomic layer deposition of ZnO transparent conducting oxides. *Appl Surf Sci.* 1997;112:216-222. <https://www.sciencedirect.com/science/article/pii/S016943329610227>
96. Chang NL, Ho-Baillie A, Wenham S, et al. A techno-economic analysis method for guiding research and investment directions for C-Si photovoltaics and its application to Al-BSF, PERC, LDSE and advanced hydrogenation. *Sustain Energy Fuels.* 2018;2(5):1007-1019.
97. Titova V, Schmidt J. Implementation of full-area-deposited electron-selective TiO_x layers into silicon solar cells. *AIP Adv.* 2018;8(12):125023.
98. Macco B, Vos MFJ, Thissen NFW, Bol AA, Kessels WMM. Low-temperature atomic layer deposition of MoO_x for silicon heterojunction solar cells. *Phys Status Solidi (RRL)-Rapid Res Lett.* 2015;9(7):393-396.
99. Vos MFJ, Macco B, Thissen NFW, Bol AA, Wmm (Erwin) kessels. *J Vac Sci Technol A.* 2015;34:01A103.
100. Ziegler J, Mews M, Kaufmann K, Schneider T, Sprafke AN, Korte L, Wehrspohn RB. Plasma-enhanced atomic-layer-deposited MoO_x emitters for silicon heterojunction solar cells. *Appl Phys A.* 2015;120(3):811-816.
101. Popovici M, Kim M-S, Tomida K, et al. Improved EOT and leakage current for metal-insulator-metal capacitor stacks with rutile TiO₂. *Microelectron Eng.* 2011;88(7):1517-1520.
102. Xie Q, Jiang Y-L, Detavernier C, et al. Atomic layer deposition of TiO₂ from tetrakis-dimethyl-amido titanium or Ti isopropoxide precursors and H₂O. *J Appl Phys.* 2007;102(8):083521.
103. Kääriäinen TO, Cameron DC, Tanttari M. Adhesion of Ti and TiC coatings on PMMA subject to plasma treatment: effect of intermediate layers of Al₂O₃ and TiO₂ deposited by atomic layer deposition. *Plasma Process Polym.* 2009;6(10):631-641.
104. Abendroth B, Moebus T, Rentrop S, et al. Atomic layer deposition of TiO₂ from tetrakis (dimethylamino) titanium and H₂O. *Thin Solid Films.* 2013;545:176-182.
105. Lin F, Nandakumar N, Dielissen B, Gortzen R, Hoex B. Excellent surface passivation of silicon at low cost: atomic layer deposited aluminium oxide from solar grade TMA. In: Conference Record of the IEEE Photovoltaic Specialists Conference; 2013:1268-1271.
106. Rontu V, Hokkanen A, Franssila S. Mechanical properties of ultrathin ALD Al₂O₃ films. In: Joint eurocvd 21-baltic ald 15 conference; 2017.
107. Mishra S, Przewdzicka E, Wozniak W, et al. Structural properties of thin ZnO films deposited by ALD under O-rich and Zn-rich growth conditions and their relationship with electrical parameters. *Materials.* 2021;14(14). URL <https://pmc/articles/PMC8307850/pmc/articles/PMC8307850/?report=abstract>
108. Chunduri S, Schmela M. TAIYANG NEWS PERC Solar Cell Technology 2016 Edition; 2016.
109. Chang NL, Ho-Baillie AWY, Vak D, Gao M, Green MA, Egan RJ. Manufacturing cost and market potential analysis of demonstrated roll-to-roll perovskite photovoltaic cell processes. *Sol Energy Mater Sol Cells.* 2018;174:314-324.
110. Lokanc M, Eggert R, Redlinger M. The availability of indium: the present, medium term, and long term, National Renewable Energy Lab. (NREL), Golden, CO (United States); 2015.

SUPPORTING INFORMATION

Additional supporting information may be found in the online version of the article at the publisher's website.

How to cite this article: Chang NL, Poduval GK, Sang B, et al. Techno-economic analysis of the use of atomic layer deposited transition metal oxides in silicon heterojunction solar cells. *Prog Photovolt Res Appl.* 2023;31(4):414-428. doi:10.1002/pip.3553